Thermal detuning of a bichromatic narrow linewidth optical cavity

L.D Bonavena, M Lequime, M Vardaro, Y Zhao, M Barsuglia, M Bawaj, A Bertolini, R Bonnand, E Capocasa, M de Laurentis, et al.

Thermal detuning of a bichromatic narrow linewidth optical cavity

L. D. Bonavena,[1,2,*,‡] M. Lequime,[3,*] M. Vardaro,[4,5,*,†] Y. Zhao,[6,*] M. Barsuglia,[6] M. Bawaj,[7,8] A. Bertolini,[5] R. Bonnand,[9] E. Capocasa,[6] M. De Laurentis,[10,11] J. Ding,[6,12] S. Di Pace,[13,14] R. Flaminio,[9] B. Garaventa,[15,16] A. Grimaldi,[17,18,§] Y. Guo,[4,5] P.-E. Jacquet,[19] A. Masserot,[9] M. Mehmet,[20] R. Passaquieti,[21,22] L. Pinard,[23] E. Polini,[9,‖] V. Sequino,[10,11] F. Sorrentino,[16] M. Tacca,[5] H. Vahlbruch,[20] and J. P. Zendri[2]

[1]*Dipartimento di Fisica e Astronomia, Università di Padova, I-35131 Padova, Italy*
[2]*INFN, Sezione di Padova, I-35131 Padova, Italy*
[3]*Aix Marseille Univ, CNRS, Centrale Med, Institut Fresnel, Marseille, France*
[4]*Maastricht University, NL-6200 MD Maastricht, Netherlands*
[5]*Nikhef, NL-1098 XG Amsterdam, Netherlands*
[6]*Université Paris Cité, CNRS, Astroparticule et Cosmologie, F-75013 Paris, France*
[7]*Università di Perugia, I-06123 Perugia, Italy*
[8]*INFN, Sezione di Perugia, I-06123 Perugia, Italy*
[9]*Université Savoie Mont Blanc, CNRS, Laboratoire d'Annecy de Physique des Particules - IN2P3, F-74000 Annecy, France*
[10]*Università di Napoli "Federico II", I-80126 Napoli, Italy*
[11]*INFN, Sezione di Napoli, I-80126 Napoli, Italy*
[12]*Corps des Mines, Mines Paris, Université PSL, Paris, France*
[13]*Università di Roma "La Sapienza", I-00185 Roma, Italy*
[14]*INFN, Sezione di Roma, I-00185 Roma, Italy*
[15]*Dipartimento di Fisica, Università degli Studi di Genova, I-16146 Genova, Italy*
[16]*INFN Genova, Sezione di Genova, I-16146 Genova, Italy*
[17]*Dipartimento di Fisica, Università di Trento, I-38123 Povo, Trento, Italy*
[18]*INFN, Trento Institute for Fundamental Physics and Applications, I-38123 Povo, Trento, Italy*
[19]*Laboratoire Kastler Brossel, Sorbonne Université, CNRS, ENS-Université PSL, Collège de France, F-75005 Paris, France*
[20]*Institut für Gravitationsphysik, Leibniz Universität Hannover and Max-Planck-Institut für Gravitationsphysik (Albert-Einstein-Institut), Callinstrasse 38, D-30167 Hannover, Germany*
[21]*Università di Pisa, I-56127 Pisa, Italy*
[22]*INFN, Sezione di Pisa, I-56127 Pisa, Italy*
[23]*Université Claude Bernard Lyon 1, CNRS, Laboratoire des Matériaux Avancés (LMA), IP2I Lyon / IN2P3, UMR 5822, F-69622 Villeurbanne, France*

(Received 29 November 2023; accepted 20 February 2024; published 11 April 2024)

In the Advanced Virgo+ interferometric gravitational-wave detector, the length control of the Fabry-Pérot cavities in the arms and of the detuned filter cavity, used for generating frequency-dependent squeezing, uses an auxiliary green beam at half of the operation laser wavelength (1064 nm). While operating the filter cavity with such a bichromatic control scheme for tens of hours, we observed that the mirror reflection phase shift of the fields at the two wavelengths responds differently to temperature changes in the mirrors, causing a change in the relative resonance condition of the two beams. In this paper we show that this thermal detuning effect can be explained by considering the thermomechanical properties of the mirror coating. Our experimental measurements are in good agreement with the theoretical predictions and allow us to drive requirements on the bicolor coating design and mirror temperature stability for long-term stable cavity control.

DOI: 10.1103/PhysRevA.109.043709

I. INTRODUCTION

Bichromatic control schemes, which use a wavelength to control the operation of a system at another wavelength, are widely used for optical resonators. In these applications the optical cavities are locked to one of the two fields' wavelength, leading to a stable detuning with respect to the cavity of the second field being kept at a fixed frequency with respect to the first. This kind of methodology is used for instance to acquire the locking of the long arm cavities in interferometric gravitational-wave detectors [1,2], for the longitudinal and angular control of the filter cavity used for the generation

*These authors contributed equally to this work.
†Corresponding address: m.vardaro@nikhef.nl
‡Present address: University of Florida, Department of Physics, 2001 Museum Road, Gainesville, Florida 32611, USA.
§Present address: QUANTOP, Danish Research Foundation Center for Quantum Optics, Niels Bohr Institute, Blegdamsvej 17, DK-2100 Copenhagen Ø, Denmark.
‖Present address: LIGO Laboratory, Massachusetts Institute of Technology, Cambridge, Massachusetts 02139, USA.

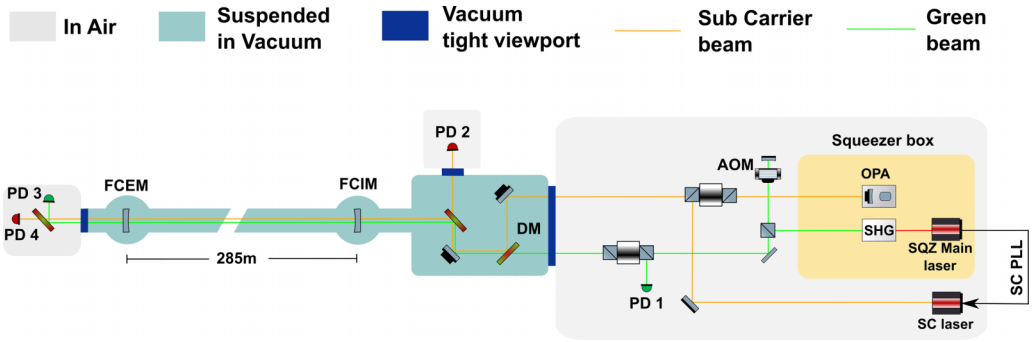

FIG. 1. Optical layout of the squeezing system showing two main environments: in-air benches and vacuum-suspended benches. The orange beam, known as a subcarrier (SC), is antiresonant in the OPA and copropagates with the squeezing beam. It is another candidate for controlling FC. PD1 provides the Pound-Drever-Hall error signal for the green FC longitudinal locking while the IR PDH signal on PD2 is used to drive the AOM for keeping the SC beam in resonance. PD3,4 are dc photodiodes in transmission of the FC for the green and the IR beams, respectively, and are used for diagnostic purposes or for triggering the locking system. The other acronyms are defined in the text.

of a frequency-dependent squeezed vacuum field [3–6] or for a weakly interacting slim particle search using optical resonators [7].

In previous work, when the two wavelengths are not exactly one the double of the other, the stability of the second field versus the cavity resonance was found to be affected by the frequency drifts of the laser sources and the cavity length [8]. Additional contributions, in the presence of an inhomogeneity of the mirror coatings, are originated from the alignment jitter of the beams.

In this paper we report a detuning fluctuation mechanism observed in the filter cavity (FC) used for the generation of the frequency-dependent squeezed (FDS) vacuum field for the gravitational-wave detector Advanced Virgo [5]. This effect is attributed to the laser wavelength temperature dependence of the mirror coating properties and has shown to be the dominating effect with respect to the aforementioned other mechanisms.

This paper is organized as follows: First, we introduce the experimental setup used for the generation of FDS in Virgo and for the measurements presented in this paper. Then, we describe the theoretical model used to estimate the thermal sensitivity of the filter cavity mirrors, and finally, we present the methodology and the results of the measurements.

The Virgo FDS states are generated via the reflection of a frequency-independent squeezed field [9,10] by an optical cavity, called the filter cavity, slightly detuned (25 Hz) with respect to the interferometer carrier [11]. The filter cavity is located inside the North tunnel of the Virgo detector, parallel to the interferometer arm. It consists of two concave mirrors, the input mirror (FCIM) and the end mirror (FCEM), spaced 285 m apart. These mirrors are seismically isolated using a scaled-down version of the Virgo superattenuator inverted pendulum and they are suspended to a marionette, from which it is possible to control the mirror orientation. A detailed description of the suspension system can be found in Ref. [12]. Longitudinal control is achieved by acting on four magnets glued to the backside of the end mirrors. The most relevant FC properties are listed in Table I while a more detailed description of the overall system can be found in Refs. [5,13].

The optical layout for the bichromatic thermal detuning measurements is shown in Fig. 1. The filter cavity is locked with the Pound-Drever-Hall (PDH) technique to the green beam (532 nm) provided by a second-harmonic generator (SHG) located inside the squeezed-light source. The frequency of this beam can be slightly modified by an acousto-optic modulator (AOM) inserted in its path. Additionally, an infrared beam, called the subcarrier (SC) beam, is injected into the optical parametric amplifier (OPA) cavity and its frequency is locked to the main squeezer laser (1064 nm) with an offset. The offset frequency is chosen in such a way that this beam is resonant in the FC and, at the same time, antiresonant in the OPA, in order to be maximally reflected by it. The reflected SC beam and the other infrared fields transmitted in the OPA are then superimposed with the green beam on a dichroic mirror (DM in Fig. 1) and copropagated

TABLE I. Summary of the filter cavity parameters. The two values indicated for the IR finesse $\mathcal{F}$ and linewidth represent the minimum and maximum value estimated in several measurement runs made at different times. FWHM stands for full width at half maximum.

Parameter	Value
Length	284.9 m
Mirror diameter	149.9 mm
Input mirror radius of curvature	556.0 m
End mirror radius of curvature	557.1 m
Input mirror flatness Φ50 mm	0.58 nm
End mirror flatness Φ50 mm	0.67 nm
Parameters for infrared	
Input mirror transmissivity	562 ppm
End mirror transmissivity	3.16 ppm
Finesse	9582–10204
Linewidth (FWHM)	51.6–54.9 Hz
Parameters for green	
Input mirror transmissivity	2.6%
End mirror transmissivity	2.7%
Finesse	117
Linewidth (FWHM)	4502 Hz

to the FC. While the green beam, which has a lower finesse, is easy to use for the lock acquisition, the SC beam is meant to be used as a final control beam for the FC, once it will operate together with the interferometer. Finally, all the laser sources are phase/frequency locked to each other and to the ultrastable Virgo main laser via phase-locked loops (PLLs). This leads to a frequency stabilization of the sources which allows to minimize the detuning fluctuation due to the mechanism reported in Ref. [8].

II. OPTICAL AND THERMAL PROPERTIES OF MIRROR COATINGS

In order to meet the optical requirements for the transmittance of the filter cavity mirrors at both wavelengths (see Table I), specific stacks of alternating silica and tantala layers (50 layers and a total thickness of 7.175 μm for the end mirror, and 36 layers and a total thickness of 4.53 μm for the input mirror) were designed and then deposited on the surface of high-quality silica substrates.

The reflection coefficient R of one of this stack, as well as the corresponding phase change ρ, can be calculated using the following general formula [14],

$$r = \frac{\tilde{n}_0 - Y_0}{\tilde{n}_0 + Y_0} = \sqrt{R}e^{i\rho}, \tag{1}$$

where $\tilde{n}_0$ is the effective index of the incident medium, and Y_0 is the complex admittance of the stack. The effective index of a medium j is defined by

$$\tilde{n}_j = \frac{1}{\eta_v \tilde{\mu}_r} \begin{cases} n_j \gamma_j / k_j & \text{for transverse electric (TE) polarization,} \\ n_j k_j / \gamma_j & \text{for transverse magnetic (TM) polarization,} \end{cases} \tag{2}$$

where η_v is the impedance of the vacuum, $\tilde{\mu}_r$ is the relative magnetic permeability of the medium j, n_j is its refractive index, k_j is the wave vector of the incident field in that medium, and γ_j is the component of that wave vector normal to the stack surface. The complex admittance of the layer j of a stack can be calculated using the following recursive formula [14],

$$Y_{j-1} = \frac{Y_j \cos\delta_j - i\tilde{n}_j \sin\delta_j}{\cos\delta_j - i(Y_j/\tilde{n}_j)\sin\delta_j}, \quad j = 1, \ldots, p, \tag{3}$$

where δ_j is the phase term associated with layer j and defined by $\delta_j = \gamma_j d_j$, where d_j is its physical thickness. The recursive formula (3) is initiated in the substrate ($Y_p = \tilde{n}_s$) where only a progressive wave is present (p is the number of layers in the stack).

At zero angle of incidence, the distinction between TE and TM polarization states disappears. Combining Eqs. (1)–(3), we can calculate the phase shift ρ as a function of wavelength for each FC mirror (end mirror FCEM or input mirror FCIM).

As the temperature of a mirror changes, the optical thickness $n_j\delta_j$ of each layer is modified according to the following general relationship [15],

$$\sigma_j = \frac{1}{\Delta T}\frac{\Delta(n_j d_j)}{n_j d_j} = \alpha_j + \beta_j - \frac{\alpha_s - \alpha_j}{1-\nu_j} \times \left\{ 2\nu_j + \frac{n_j^2}{2}[(1-\nu_j)p_{11} + (1-3\nu_j)p_{12}] \right\}, \tag{4}$$

where σ_j is the relative thermal sensitivity of the optical thickness of the layer j, α_j (or α_s) is the coefficient of thermal expansion of layer j (or substrate), β_j is the thermo-optic coefficient of that layer, ν_j is its Poisson's ratio, and p_{11} and p_{12} are two components of the elasto-optic tensor of the material of layer j. The thermally induced change in the optical thickness of the layers modifies the spectral dependence of the phase shift ρ of the stack and, accordingly, the frequency detuning between green and infrared wavelengths.

The definition of the numerical values for all these relevant parameters (α_j, β_j, ν_j, p_{11}, and P_{12}) in the case of silica and tantala coatings is not straightforward, but by combining published values for thin films and/or for bulk [16,17], and data from our own work [18,19], we have arrived at the mean values listed in Table II, whose dispersion is estimated approximately to ±15%.

By adding the thermal expansion coefficient of the silica substrate ($\alpha_s = 5.1 \times 10^{-7}\,^\circ\mathrm{C}^{-1}$), we can calculate the thermal sensitivity σ of the two coating materials, namely

$$\sigma_{\mathrm{SiO2}} = 7.5 \times 10^{-6}\,^\circ\mathrm{C}^{-1}, \quad \sigma_{\mathrm{Ta2O5}} = 10.8 \times 10^{-6}\,^\circ\mathrm{C}^{-1}.$$

We can now simulate the effect of a temperature change of 1 °C on the value of the phase shift ρ at the two wavelengths of the bichromatic scheme, and then derive the corresponding thermal sensitivity (1 for green, 2 for infrared).

The green wavelength is used to lock the cavity at resonance. The change in cavity length L induced by a change in temperature of one of the FC mirrors is thus given by

$$\Delta L = \frac{\partial L}{\partial T}\Delta T = -\frac{c}{4\pi f_1}\frac{\partial \rho_1}{\partial T}\Delta T. \tag{5}$$

Furthermore, the thermal detuning of the infrared frequency f_2 is given by

$$\Delta f_2 = \frac{\partial f_2}{\partial T}\Delta T = -\frac{c}{4\pi L}\left\{ \frac{\partial \rho_2}{\partial T} + \frac{4\pi f_2}{c}\frac{\partial L}{\partial T} \right\}\Delta T. \tag{6}$$

By combining (5) and (6) and using $f_1 = 2f_2$, we finally get the sensitivity of the bichromatic detuning to the temperature change of one FC mirror, which is given by the following

TABLE II. Thermomechanical layer properties (α and β in $^\circ\mathrm{C}^{-1}$).

Parameter	Silica	Tantala
Thermal expansion coefficient α	2.1×10^{-6}	3.4×10^{-6}
Thermo-optic coefficient β	3.9×10^{-6}	4.0×10^{-6}
Poisson coefficient ν	0.11	0.24
Elasto-optic tensor p_{11} term	0.121	0.068
Elasto-optic tensor p_{12} term	0.270	0.164

TABLE III. Thermal sensitivity of the mirror properties.

FC Mirror	$\partial\rho_1/\partial T$ (μrad/°C)	$\partial\rho_2/\partial T$ (μrad/°C)	S_T (Hz/°C)
FCEM	3194	157	120
FCIM	1414	58	54

relationship,

$$S_T = \frac{c}{4\pi L}\left\{\frac{1}{2}\frac{\partial\rho_1}{\partial T} - \frac{\partial\rho_2}{\partial T}\right\}, \tag{7}$$

where L is the length of the filter cavity (284.9 m). The numerical values of all these thermal sensitivities are summarized in Table III.

Bichromatic thermal detuning measurement methodology and results

In the set of measurements shown, a drift in mirror temperatures was artificially induced by changing the temperature set point of the hosting room by approximately 1.5 °C while keeping the room temperature of the other mirror constant. The temperature step is limited to 1.5 °C to ensure the mirror's longitudinal and angular controls to be used within their operating ranges. Throughout the measurement process, the filter cavity was locked with the green beam, while the SC beam was precisely kept in resonance within the FC by adjusting the frequency of the AOM. As a result, the frequency offset applied to the AOM serves as a direct indicator of how the difference in resonance frequency between the two wavelengths evolves over time. Since there are no thermometers mounted directly on the mirrors, their temperature is estimated from the thermistor positioned on the ring heaters which are installed around the mirrors at a distance of a few millimeters [20]. To overcome the lack of knowledge of the different thermalization times of the mirror and the ring heater, in our analysis we selected the data where both the ring heater temperature and the detuning frequency exhibit a constant slope over time. In these conditions the temperature rate change of the ring heater is expected to match that of the mirror regardless of any constant thermal delay between them.

The measurements of the bichromatic thermal detuning of the filter cavity versus temperature are shown in Figs. 2 and 3. For both figures, the mirror temperature trend is shown in the upper subplot. In these two measurements, we keep one mirror at the stabilized temperature of the room and we induced on the other a temperature variation with a rate of about 0.1 K/h.

For the selected data type the filter cavity detuning rate $\Delta\nu_{\rm FC}/\Delta t$ is expected to scale as a function of the "input" and "end" mirrors' temperature change rate $\Delta T_{\rm FCIM,FCEM}/\Delta t$ as

$$\frac{\Delta\nu_{\rm FC}}{\Delta t} = S_{T_{\rm FCIM}}\frac{\Delta T_{\rm FCIM}}{\Delta t} + S_{T_{\rm FCEM}}\frac{\Delta T_{\rm FCEM}}{\Delta t}, \tag{8}$$

where $S_{T_{\rm FCIM(FCEM)}}$ is the input (output) mirror bichromatic detuning temperature sensitivity [see Eq. (7)]. In order to estimate separately these two coefficients we selected the data region where one of the mirror temperatures is most stabilized while the other is free to move. In addition, to avoid some obvious noise in the measurement, the selected region avoids

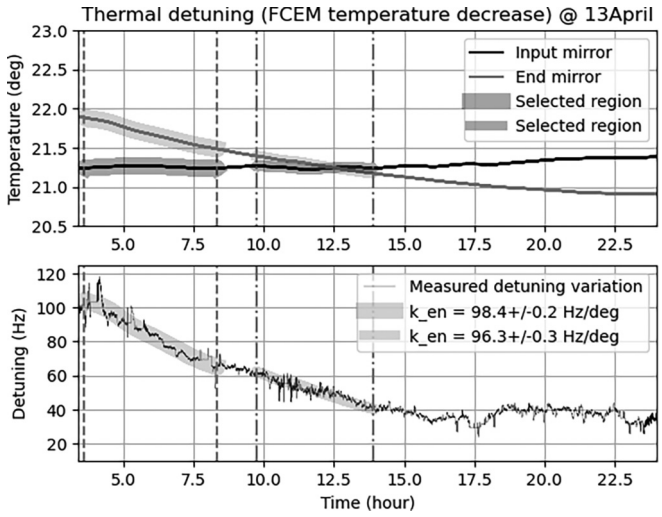

FIG. 2. Measurement of bichromatic thermal detuning by decreasing the filter cavity end mirror temperature.

spikes in the measured detuning variation. These selected regions are highlighted in the corresponding plot.

For the selected data set, the estimated detuning frequency (lower subplot in Figs. 2 and 3) is linearly interpolated against the temperature drift of the mirrors. The systematic error $\delta S_{T_{\rm FCIM(FCEM)}}$ deriving from the assumption of having a mirror perfectly stabilized in temperature is estimated as

$$\delta S_{T_{\rm FCIM(FCEM)}} = S_{T_{\rm FCEM(FCIM)}}\frac{\delta(\Delta T_{\rm FCEM(FCIM)}/\Delta t)}{\Delta T_{\rm FCIM(FCEM)}/\Delta t}, \tag{9}$$

where $\delta(\Delta T_{\rm FCEM(FCIM)})$ is the residual temperature rate error of the temperature-stabilized mirror.

The average of fitting results in Figs. 2 and 3 gives a detuning rate $S_{T_{\rm FCIM}} = 51 \pm 7$ Hz/°C and $S_{T_{\rm FCEM}} = 97 \pm 14$ Hz/°C for FCIM and FCEM, respectively. Considering the

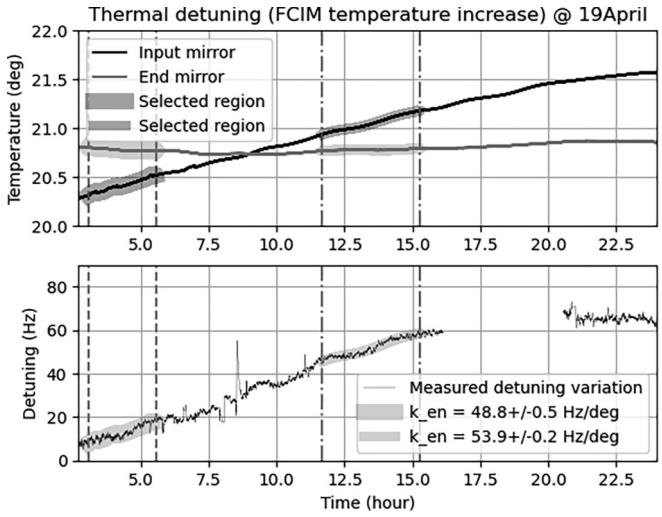

FIG. 3. Measurement of bichromatic thermal detuning by increasing the filter cavity input mirror temperature. There are some data not shown in the plot since the cavity was not properly locked at that moment.

uncertainty of their estimates, these experimental values agree with the theoretical predictions reported in Table III.

In conclusion, this work shows the need of a tight constraint on the mirrors' temperature stability in order to keep a stable detuning, when the control bichromatic scheme is used. This might not be particularly worrying for Virgo, as a different control scheme based on the IR SC should be eventually used for the control of the FC, once it will be coupled with the interferometer [13]. Moreover, the theoretical model described and validated in this work can help in the design of next-generation coating stacks that are less demanding in terms of the temperature stabilization in case a multiwavelength control scheme is envisaged.

ACKNOWLEDGMENTS

The authors gratefully acknowledge the support of the Max Planck Society, Leibniz Universität Hannover and Deutsche Forschungsgemeinschaft (DFG, German Research Foundation) through project Grant No. VA 1031/1-1 and Germany's Excellence Strategy – EXC-2123 QuantumFrontiers – 390837967 for the construction, installation, and operation of the squeezed-light source. The authors are also grateful to the Genova, Napoli, Padova, Perugia Roma I, and Trento Univeristies and sections of the Italian National Institute of Nuclear Physics (INFN) for the realization of the squeezed vacuum source bench among with the PLLs and the diagnostic homodyne electronics. We also thank the Particle Physics Laboratory of Annecy (LAPP) (F) for providing the suspended optical benches, the clean rooms around them, and the data acquisition system, the Dutch National Institute for Atomic Physics (Nikhef) for supplying the cavity vacuum system, the mechanical suspension for both the in-vacuum benches and the cavity mirrors, and the rf quadrant photodiode readout, the Laboratoire des Materiaux Avancés (LMA) of Lyon (F) for the realization of the optical coatings, the Institute of Cosmos Sciences (ICCUB) for providing the in-vacuum position-sensitive detector, the Institute of High Energy Physics (IFAE) of Barcelona (E) for the realization and the installation of the vacuum baffle, the Rome Tor-Vergata group for the ring heaters, the Perugia group for the assembly of the mirrors, and the Napoli group for optical lever position sensors. Special thanks go to the staff of the European Gravitational Observatory (EGO) for the relevant role in the logistics, in the implementation of the structural changes, in the electronics cabling, in the development of customized electronics, and in the supply of the low-loss Faraday isolators. This work has been also supported by LabEx UnivEarthS (ANR-10-LABX-0023 and ANR-18-IDEX-0001).

[1] T. Akutsu, M. Ando, K. Arai, Y. Arai, S. Araki, A. Araya, N. Aritomi, Y. Aso, S. Bae, Y. Bae *et al.*, Class. Quantum Grav. **37**, 035004 (2020).

[2] A. Staley, D. Martynov, R. Abbott, R. Adhikari, K. Arai, S. Ballmer, L. Barsotti, A. Brooks, R. DeRosa, S. Dwyer *et al.*, Class. Quantum Grav. **31**, 245010 (2014).

[3] Y. Zhao, N. Aritomi, E. Capocasa, M. Leonardi, M. Eisenmann, Y. Guo, E. Polini, A. Tomura, K. Arai, Y. Aso *et al.*, Phys. Rev. Lett. **124**, 171101 (2020).

[4] L. McCuller, C. Whittle, D. Ganapathy, K. Komori, M. Tse, A. Fernandez-Galiana, L. Barsotti, P. Fritschel, M. MacInnis, F. Matichard *et al.*, Phys. Rev. Lett. **124**, 171102 (2020).

[5] F. Acernese *et al.* (Virgo Collaboration), Phys. Rev. Lett. **131**, 041403 (2023).

[6] D. Ganapathy *et al.* (LIGO O4 Detector Collaboration), Phys. Rev. X **13**, 041021 (2023).

[7] R. Bähre, B. Döbrich, J. Dreyling-Eschweiler, S. Ghazaryan, R. Hodajerdi, D. Horns, F. Januschek, E.-A. Knabbe, A. Lindner, D. Notz *et al.*, J. Instrum. **8**, T09001 (2013).

[8] Y. Zhao, E. Capocasa, M. Eisenmann, N. Aritomi, M. Page, Y. Guo, E. Polini, K. Arai, Y. Aso, M. van Beuzekom *et al.*, Phys. Rev. D **105**, 082003 (2022).

[9] M. Mehmet and H. Vahlbruch, Class. Quantum Grav. **36**, 015014 (2019).

[10] F. Acernese *et al.* (Virgo Collaboration), Phys. Rev. Lett. **123**, 231108 (2019).

[11] H. J. Kimble, Y. Levin, A. B. Matsko, K. S. Thorne, and S. P. Vyatchanin, Phys. Rev. D **65**, 022002 (2001).

[12] R. C. Walet, Ph.D. thesis, Vrije Universiteit Amsterdam, 2022.

[13] F. Acernese *et al.*, Advanced Virgo Plus Phase, Technical Report No. VIR-0596A-19 (2019).

[14] C. Amra, M. Lequime, and M. Zerrad, *Electromagnetic Optics of Thin-Film Coatings: Light Scattering, Giant Field Enhancement, and Planar Microcavities* (Cambridge University Press, Cambridge, UK, 2021).

[15] M. Lequime, Proc. SPIE **5250**, 302 (2004).

[16] E. Çetinörgü, B. Baloukas, O. Zabeida, J. E. Klemberg-Sapieha, and L. Martinu, Appl. Opt. **48**, 4536 (2009).

[17] G. H. Ogin, Ph.D. thesis, California Institute of Technology, 2013.

[18] R. Parmentier and M. Lequime, Opt. Lett. **28**, 728 (2003).

[19] S. Michel, Ph.D. thesis, Aix-Marseille Université, 2008.

[20] I. Nardecchia, Y. Minenkov, M. Lorenzini, L. Aiello, E. Cesarini, D. Lumaca, V. Malvezzi, F. Paoletti, A. Rocchi, and V. Fafone, Class. Quantum Grav. **40**, 055004 (2023).